Mechanism of Activation of a G Protein-coupled Receptor, the Human Cholecystokinin-2 Receptor

THE JOURNAL OF BIOLOGICAL CHEMISTRY VOL. 282, NO. 39, pp. 28779–28790, September 28, 2007

Mechanism of Activation of a G Protein-coupled Receptor, the Human Cholecystokinin-2 Receptor*

Received for publication, January 12, 2007, and in revised form, June 21, 2007 Published, JBC Papers in Press, June 28, 2007, DOI 10.1074/jbc.M700349200

Esther Marco[1,2], **Magali Foucaud**[2], **Ingrid Langer**[1,3], **Chantal Escrieut, Irina G. Tikhonova**[1], **and Daniel Fourmy**[4]

From INSERM, Unit 858, Institut Fédératif de Recherche, 31432 Toulouse, France and the Université de Toulouse 3, 31062 Toulouse, France

G protein-coupled receptors (GPCRs) represent a major focus in functional genomics programs and drug development research, but their important potential as drug targets contrasts with the still limited data available concerning their activation mechanism. Here, we investigated the activation mechanism of the cholecystokinin-2 receptor (CCK2R). The three-dimensional structure of inactive CCK2R was homology-modeled on the basis of crystal coordinates of inactive rhodopsin. Starting from the inactive CCK2R modeled structure, active CCK2R (namely cholecystokinin-occupied CCK2R) was modeled by means of steered molecular dynamics in a lipid bilayer and by using available data from other GPCRs, including rhodopsin. By comparing the modeled structures of the inactive and active CCK2R, we identified changes in the relative position of helices and networks of interacting residues, which were expected to stabilize either the active or inactive states of CCK2R. Using targeted molecular dynamics simulations capable of converting CCK2R from the inactive to the active state, we delineated structural changes at the atomic level. The activation mechanism involved significant movements of helices VI and V, a slight movement of helices IV and VII, and changes in the position of critical residues within or near the binding site. The mutation of key amino acids yielded inactive or constitutively active CCK2R mutants, supporting this proposed mechanism. Such progress in the refinement of the CCK2R binding site structure and in knowledge of CCK2R activation mechanisms will enable target-based optimization of nonpeptide ligands.

The superfamily of G protein-coupled receptors (GPCRs)[5] represents a large and diverse family of seven transmembrane helix proteins. Because they are involved in all physiological processes, GPCRs are targeted by 50% of marketed drugs. However, these drugs address only a small fraction of the GPCR repertoire. GPCRs represent a major focus in functional genomics programs and drug development research, but their important potential as drug targets contrasts strongly with the very limited data available regarding their activation mechanism. The activation of GPCRs is generally explained by the extended ternary complex model whereby the population of receptors exists as an equilibrium between inactive and active states (1). According to this model, the active conformation of the receptor may be stabilized or induced by agonists. The extended ternary complex model for GPCRs is based on and sustained by the discovery of engineered constitutively active mutants, namely mutants that produce ligand-independent signaling (1). Constitutively active GPCR mutants naturally exist in humans and can cause diseases (2). Interestingly, constitutive GPCR signaling can be inhibited or attenuated by a class of therapeutic agents named inverse agonists (2, 3).

The cholecystokinin (CCK)-2 receptor (CCK2R), previously named the CCKB/gastrin receptor, belongs to family I of GPCRs, which includes rhodopsin (4–6). It binds both cholecystokinin and gastrin, two structurally related neuropeptides with similar high affinities. CCK2R is expressed in the central nervous system and in the gut, where it represents the predominant CCK receptor subtype. CCK2R mediates a wide spectrum of CCK- and gastrin-induced biological effects, including anxiety, pain perception, gastric acid secretion, growth, and differentiation of the gastric mucosa (4, 7). Converging studies have documented that activation of wild-type CCK2R and/or expression of a constitutively active variant may contribute to human diseases (8, 9). These new findings have generated considerable interest in the identification of antagonists of CCK2R. To date, a large panel of chemically distinct CCK2R antagonists have been discovered and used to assess the functions mediated by CCK2R in animals and humans (10). Furthermore, several of these compounds have reached clinical evaluation stages for indications such as anxiety and panic disorders, sleep disorders, drug dependence, pain, gastroesophagus reflux, and gastric secretion disorders (10). However, some reference molecules believed to be pure antagonists turned out to be endowed with some agonist activity in the stomach and pancreas as well as cells expressing CCK1R or CCK2R (11–13). On the other hand, reports on the expression of constitutively active receptors in digestive cancers and on potential therapeutic relevance for neuroendocrine tumors highlighted the need to identify inverse agonists able to reverse basal constitutive activity of CCK2R (14).

Target structure-based design of new ligands requires iden-

* This work was supported in part by Association pour la Recherche contre le Cancer Grants ARC 3282 and 3756. The costs of publication of this article were defrayed in part by the payment of page charges. This article must therefore be hereby marked "*advertisement*" in accordance with 18 U.S.C. Section 1734 solely to indicate this fact.
[1] Supported by fellowships from the "Fondation pour la Recherche Medicale."
[2] These two authors contributed equally to this work.
[3] "Chargée de Recherches" from the Fonds National de la Recherche Scientifique, Belgium.
[4] To whom correspondence should be addressed: IFR 31, Institut Louis Bugnard, BP 84225, Unité 858, 31432 Toulouse cedex 4, France. E-mail: fourmyd@toulouse.inserm.fr.
[5] The abbreviations used are: GPCR, G protein-coupled receptor; CCK, cholecystokinin; CCK2R, cholecystokinin-2 receptor; MD, molecular dynamics; DMEM, Dulbecco's modified Eagle's medium; Ins-P, inositol phosphate; TMD, targeted molecular dynamics; r.m.s., root mean square.

tification of the receptor binding site and determination of the activation mechanism. Toward this aim, our group has progressively delineated the binding site of CCK2R using site-directed mutagenesis combined with molecular modeling approaches (15–17). We identified several aromatic residues belonging to a network presumably critical for CCK2R activation (18). In this last study, differential motion of amino acid side chains within the binding pocket was observed upon *in silico* binding of different nonpeptide ligands that present distinct pharmacological features. Nevertheless, due to the intrinsic limitations of the modeling procedure used, no global change in CCK2R conformation was observed (18).

The aim of the present study was to increase our knowledge of the molecular mechanisms whereby CCK2R is activated. For this purpose, three-dimensional models of inactive and active CCK2R were constructed on the basis of available structural data. These modeled structures were studied using unrestrained molecular dynamics simulations (MDs) in an explicit water-lipid environment. By comparing averaged modeled structures, we identified changes in the relative positions of helices and networks of interacting residues expected to stabilize either active or inactive states of CCK2R. The activation mechanism of the receptor was further investigated using targeted molecular dynamics simulations and site-directed mutagenesis.

EXPERIMENTAL PROCEDURES

Molecular Modeling

Modeling of the "Inactive" CCK2R Structure (CCK2R°)—The structure of bovine rhodopsin (Protein Data Bank code 1U19) crystallized in the dark was used as structural template for the homology modeling of the CCK2R receptor (19). Alignment of human CCK2R sequence and bovine rhodopsin sequences was carried out using the ClustalW multiple alignment program (20). Loops connecting transmembrane helices were modeled using the *ab initio* modeling program MODLOOP (21). The third intracellular loop was not included in the modeled structure. The crude homology model was refined using AMBER8 (available on the World Wide Web) by means of 1000 steps of steepest descent energy minimization followed by 2000 steps of conjugate gradient energy minimization while all Cα carbons were harmonically restrained to their initial positions. This procedure allowed readjustment of covalent bonds and van der Waals contacts without changing the overall conformation of the protein. The model was then refined by molecular dynamics simulations in an explicit lipid bilayer. It was neutralized by the addition of 17 chloride ions and placed in a rectangular box ($\sim$78 $\times$ 80 $\times$ 78 Å in size) containing a lipid bilayer (153 molecules of palmitoyloleoylphosphatidylcholine and 8708 molecules of water in addition to the receptor structure), resulting in a final density of 1.0 g/cm. MD simulations at 300 K and constant pressure (1 atm) with anisotropic scaling were then run for 1ns using the SANDER module in AMBER 8. The cut-off distance for the nonbonded interactions was 9 Å, and periodic boundary conditions were applied. Electrostatic interactions were represented using the smooth particle mesh Ewald method with a grid spacing of $\sim$1 Å. The coupling constants for the temperature and pressure baths were 1.0 and 0.2 ps, respectively. SHAKE was applied to all bonds involving hydrogen, and an integration step of 2 fs was used throughout. The nonbonded pair list was updated every 10 steps. The simulation protocol involved a series of progressive energy minimizations followed by a 20-ps heating phase and a 250-ps equilibration period, during which secondary structure restraints were applied to the transmembrane helices. These restraints were removed during the following 750 ps of data collection. System coordinates were saved every 2 ps for analysis.

Modeling of the "Active" CCK2R Structure (CCK2R)*—The CCK2R° homology model obtained from the rhodopsin crystal was not directly suitable for docking purposes, because the ligand-binding pocket of inactive rhodopsin is remarkably narrow (19). We therefore refined the rhodopsin-based CCK2R° model in order to obtain a model of active CCK2R. Since it has been proposed that the conserved tryptophan belonging to the CWPFF motif in helix VI changes its orientation with respect to the membrane plane during activation, being perpendicular in the inactive form and parallel in the active form, the side chain of Trp-6.48 was manually rotated to adopt the latter conformation (22, 23). We then docked CCK4 into this crude model, taking into account all amino acids and key interactions identified in the course of binding site studies (15, 24, 25) and ran steered molecular dynamics simulations. In fact, steered molecular dynamics were first performed in the presence of CCK4, because contacts were only available for the last four residues of CCK, which correspond to the ligand binding region. Then the N-terminal extension of CCK was added. The simulation was performed *in vacuo* with a small spherical shell of 450 TIP3P water molecules centered around His-207. The radius of this water shell was 20 Å, ensuring the solvation of the extracellular portion of the helices and the extracellular loops. These water molecules were first energy-minimized, and then waters and protein residues were allowed to relax. In each case, 1000 steps of steepest descent were followed by 2000 steps of conjugate gradient energy minimization. The final coordinate sets were used as input for the subsequent steered MD simulations. SHAKE was used for all bonds, and the integration time step was 2 fs. The cut-off was 12 Å, and a distance-dependent dielectric function was used. The list of nonbonded pairs was updated every 25 steps, and coordinates were saved every 2 ps for further analysis.

The second run of 500-ps steered molecular dynamics simulations consisted of applying distance constraints by means of a harmonic potential as indicated in Table 1. The Cα carbons of helices I–III were restrained by positional constraints of 1 kcal/mol $\times$ Å during all of the simulation.

Once the desired distances were attained, CCK4 was substituted by CCK in the binding site. The final model was then refined by 1 ns of unrestrained MDs in an explicit lipid bilayer using the protocol described above for the CCK2R°. Finally, CCK was removed from the complex, and the free active conformation of CCK2R (CCK2R*) was also simulated by 1 ns of MD in a lipid environment. Although CCK2R* is energetically less stable than CCK2R°, the CCK2R* model did not relax back to CCK2R° during MD, because this back conversion would

require a microsecond time scale and could not be observed with MD simulations in the nanoseconds time scale.

In Silico Conversion of CCK2R° to CCK2R Using Targeted Molecular Dynamics Simulations*

The targeted molecular dynamics (TMD) approach used the standard implementation recently incorporated into AMBER (version 8.0) (available on the World Wide Web), which allows solvent molecules to move freely and follow the dynamics of the protein. A restraint was defined in terms of a mass-weighted r.m.s. superposition to the final reference structure (target, CCK2R*) and applied in the force field as an extra harmonic potential energy term of the following form,

$$E = 0.5kr \times N(\text{r.m.s.d.} - \text{t.r.m.s.d.})^2 \quad \text{(Eq. 1)}$$

where E is the biasing potential energy in kcal/mol during the TMD simulation, kr is the force constant, N is the number of atoms, r.m.s.d. is the root mean square deviation from the target structure, and t.r.m.s.d. is the desired root mean square deviation value. The initial value of the desired root mean square deviation was set as the root mean square deviation between the initial and target structures (CCK2R° and CCK2R*, respectively), and during the simulation, the desired root mean square deviation value was gradually decreased to 0. Only the heavy atoms of the protein were considered in the r.m.s. definition. A force constant of 0.50 kcal/mol × Å over 0.5 ns appeared sufficient to find a low energy path leading from the simulated structure to the target structure.

Site-directed Mutagenesis of CCK2R and Transfection of COS-7 Cells

All mutant receptor cDNAs were constructed by oligonucleotide-directed mutagenesis (QuikChange™ site-directed mutagenesis kit; Stratagene) using human CCK2R cDNAs cloned in the pRFNeo vector as template. The presence of desired and the absence of undesired mutations were confirmed by automated sequencing of the complete CCK2R coding sequence (Applied Biosystems). COS-7 cells (1.5×10^6) were plated onto 10-cm culture dishes and grown in Dulbecco's modified Eagle's medium (DMEM) containing 5% fetal calf serum in a 5% CO_2 atmosphere at 37 °C. After overnight incubation, cells were transfected with 1 μg/plate of pRFNeo vectors containing the cDNA for the wild-type or mutated CCK2 receptors, using a modified DEAE-dextran method. Cells were transferred to 24-well plates 24 h after transfection at a density of 150,000 cells/well for inositol phosphate determination and 5000–10,000 cells/well for binding assays.

Inositol Phosphate Production Determination

Approximately 24 h after transfer to 24-well plates and following overnight incubation in DMEM containing 2 μCi/ml myo-2-[^{3}H]inositol (specific activity 10–25 Ci/ml; PerkinElmer Life Sciences), transfected cells were washed with DMEM and incubated for 30 min in 1 ml/well DMEM containing 20 mM LiCl at 37 °C. Cells were washed with Ins-P buffer at pH 7.45: phosphate-buffered saline containing 135 mM NaCl, 20 mM HEPES, 2 mM $CaCl_2$, 1.2 mM $MgSO_4$, 1 mM EGTA, 10 mM LiCl, 11.1 mM glucose, and 0.5% bovine serum albumin. Cells were then incubated for 60 min at 37 °C in 0.3-ml Ins-P buffer alone or with CCK in the presence of increasing concentrations of synthetic ligands. Reactions were stopped by adding 1 ml of methanol/HCl to each well, and contents were transferred to a column (Dowex AG 1-X8, formate form; Bio-Rad) for the determination of Ins-P. Columns were washed twice with 3 ml of distilled water and twice with 2 ml of 5 mM sodium tetraborate, 60 mM sodium formate. The content of each column was eluted by the addition of 2 ml of 1 M ammonium formate, 100 mM formic acid. Radioactivity of 1 ml of the eluted fraction was evaluated using a liquid scintillation counter (Packard Instrument Co.). Values for Ins-P accumulation were normalized to a constant number of expressed receptors (1 pmol) and were expressed as -fold number of the basal value achieved with the wild-type CCK2R. Mock cells were transfected with a pRFNeo noncoding vector.

Receptor Binding Assay

Approximately 24 h after transfer of transfected cells to 24-well plates, the cells were washed with phosphate-buffered saline, pH 7.4, containing 0.1% bovine serum albumin and incubated for 60 min at 37 °C in 0.3 ml DMEM containing 0.1% bovine serum albumin with an appropriate concentration of high pressure liquid chromatography-purified ^{125}I-BH-(Thr,Nle)-CCK9 (specific activity 1600–2000 Ci/mmol) in the presence or absence of unlabeled CCK. Cells were washed twice with cold phosphate-buffered saline, pH 7.4, containing 2% bovine serum albumin, and cell-associated radioligand was collected by cell lysis with 0.1 N NaOH. The radioactivity was directly counted in a γ counter (Auto-Gamma; Packard Instrument Co.). Receptor density (B_{max}) and K_d were calculated from homologous ^{125}I-BH-(Thr,Nle)-CCK9 competition binding experiments using Ligand software (Kell, Cambridge, UK). K_i values were calculated using the nonlinear curve fitting software GraphPad Prism (San Diego, CA).

RESULTS

Modeled Structure of Active CCK2R (CCK2R)*—Because CCK2R is a member of the family I of rhodopsin-like GPCRs, the three-dimensional model of the inactive state of the CCK2R (CCK2R°) was constructed by homology modeling using coordinates from the inactive rhodopsin crystal isolated in the dark (19). To obtain CCK2R*, the agonist·CCK2R complex was modeled (Fig. 1). The procedure of modeling, which is described in detail under "Experimental Procedures," included the following main steps: rotation of conserved Trp-6.48 side chain (22); docking of CCK4 followed by steered molecular dynamics simulation in vacuum; steered molecular dynamics simulation based on constrained distances indicated in Table 1 and derived from published data on GPCR activation; and refinement in a lipid bilayer (see Table 1 for references).

As illustrated in Fig. 2, after the equilibration period, progression of the r.m.s. deviations of the coordinates of the Cα atoms relative to the average structure showed a notably stable behavior, reflecting that the overall architecture of the protein was preserved for the whole length of the simulation for both CCK2R° and the CCK2R*·CCK complex. Furthermore,

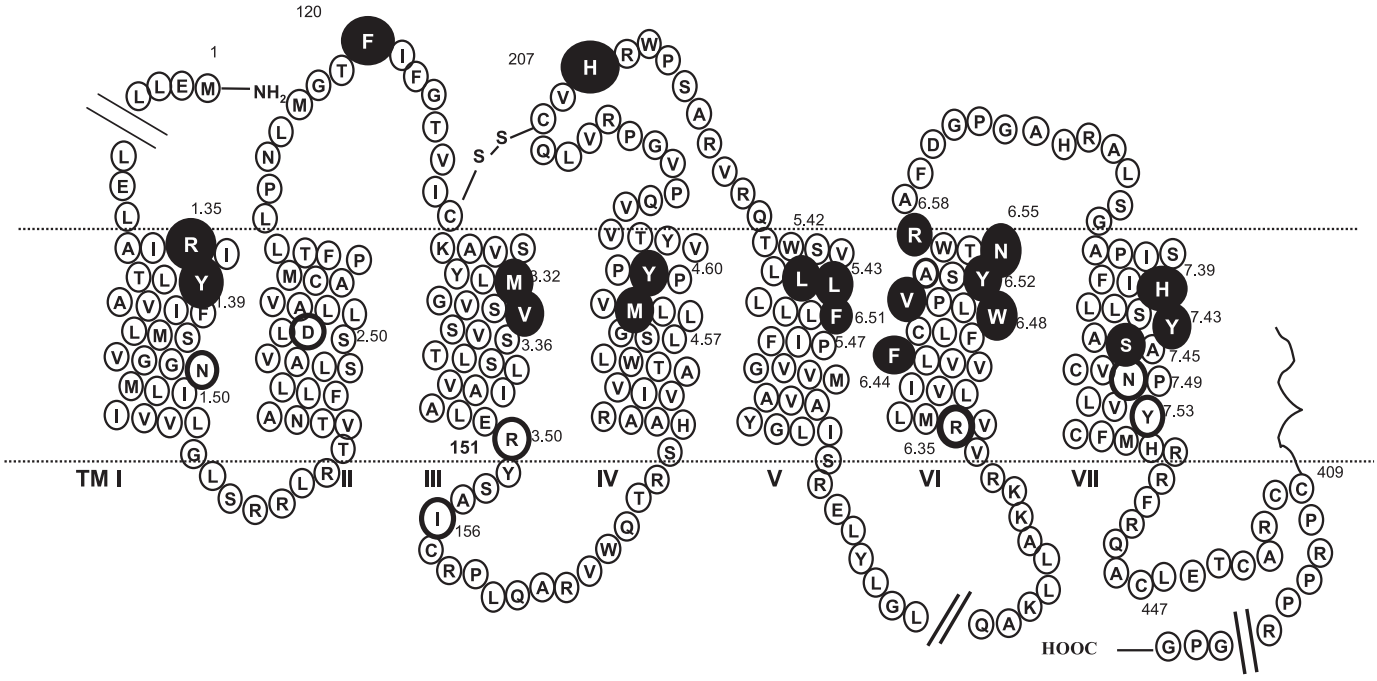

FIGURE 1. ***Serpentine representation* of human CCK2R.** Main amino acids of the CCK2R binding site (indicated as *white letters* in *filled black circles*) as well as those between which constraints were applied (indicated as *black letters* in *empty circles*; see Table 1) during CCK2R* modeling are *numbered*.

TABLE 1

Distances between amino acids used for generation of the CCK2R* model

The desired values are given in parentheses.

Distances	CCK2R*·CCK complex[a]	Reference
	Å	
Forced during the steered molecular dynamics simulation		
Tyr-4.60 OH CCK-Phe O (2.8–3.2 Å)[b]	3.1 ± 0.3	16
Asn-6.55 OD1 CCK-Phe N2 (2.8–3.2 Å)[b]	2.9 ± 0.1	16
Arg-6.58 NH1 CCK-Asp-8 OD1 (2.8–3.2 Å)[b]	2.8 ± 0.1	16
His-207 NE2 CCK-Asp-8 OD1 (2.8–3.2 Å)[b]	2.9 ± 0.1	16
Met-4.57 SD centroid CCK-Phe centroid (5 Å)[b]	5.6 ± 0.5	24
Ile-156 Cα Arg-6.35 Cα (18.5 Å)[c]	18.3 ± 0.5	47
Arg-3.50 Cα Tyr-7.53 Cα (19 Å)[c]	18.2 ± 0.5	48
Tyr-7.53 OH Asn-1.50 OD1[d]	2.8 ± 0.1	49
Asp-2.50 OD2 Asn-1.50 ND2[d]	2.9 ± 0.1	49
Asp-2.50 OD2 Asn-7.49 ND2[d]	3.0 ± 0.2	49
Nonforced		
His-7.39 centroid CCK-SO_3H(Tyr) centroid	4.2 ± 0.3	
Tyr-4.60 centroid CCK-Phe centroid	5.4 ± 0.4	
Tyr-7.43 centroid CCK-Trp centroid	5.0 ± 0.3	

[a] Mean distances ± S.D. obtained from the production part of the MD in an explicit membrane.
[b] Applied during the first 500 ps of the simulations. The force constant was fixed to 10 kcal mol^{-1} $Å^{-2}$.
[c] Applied in the successive 500 ps of the simulations. In this case, the force constant was progressively increased 2 kcal mol^{-1} $Å^{-2}$ during five consecutive runs of 100 ps each.
[d] Applied in the last 100 ps.

inter-Cα distances used during steered molecular dynamics were maintained in the absence of external restraints (Table 1). As a consequence of CCK docking and molecular dynamics applied to the complex, the binding pocket of the initial rhodopsin-based model (CCK2R°) was enlarged to snugly accommodate CCK in a position that was in agreement with site-directed mutagenesis data (see Table 3) (see Table 1 for references). Indeed, the CCK binding pocket was mainly formed by residues from transmembrane helices (Figs. 1 and 3). Sulfated CCK-Tyr was well engaged by two hydrogen bonds with Arg-1.35 and Tyr-1.39 and by stacking interactions with His-7.39. The CCK-tryptophan was located in the hydrophobic/aromatic pocket formed by residues from helices III, VII, and the first extracellular loop. The indole moiety of this residue established aromatic contacts with Tyr-7.43 and hydrophobic contacts with Phe-120 in the first extracellular loop and His-7.39. The CCK-methionine residue was placed between helix VI and helix VII interacting with Val-6.51 and the Cα carbon of Ser-7.45. The phenylalanine ring was located in a hydrophobic/aromatic pocket composed of residues from different helices: Val-3.36, Met-4.57 and Tyr-4.60, Leu-5.46, and Val-6.51 and Tyr-6.52. The aspartic acid residue accepted hydrogen bonds from His-207 in the second extracellular loop and the guanidinium group of Arg-6.58. The carbonyl group of CCK amide accepted a hydrogen bond from Tyr-4.60 hydroxyl oxygen, and CCK nitrogen amide donated a hydrogen to Asn-6.55 carbonyl amide. The fact that all of these intermolecular interactions were maintained after the equilibration period confirmed the stability of the modeled complex (Table 1). After the removal of CCK, the unbound CCK2R* was inserted into an explicit lipid bilayer and subjected to molecular dynamics simulations, resulting in a stable trajectory (Fig. 2) and yielding the refined CCK2R* model.

*Comparison of the Modeled Structures of CCK2R° and CCK2R**—In order to investigate the activation mechanism of CCK2R, we first compared averaged structures of refined CCK2R° and CCK2R* models. Actually, we assumed that CCK2R naturally exists in an equilibrium between receptors in the inactive (CCK2R°) and active state (CCK2R*) and that specific intramolecular networks stabilize each conformation. In support of this assumption, we previously showed that human wild-type CCK2R presents some degree of constitutive activity (18).

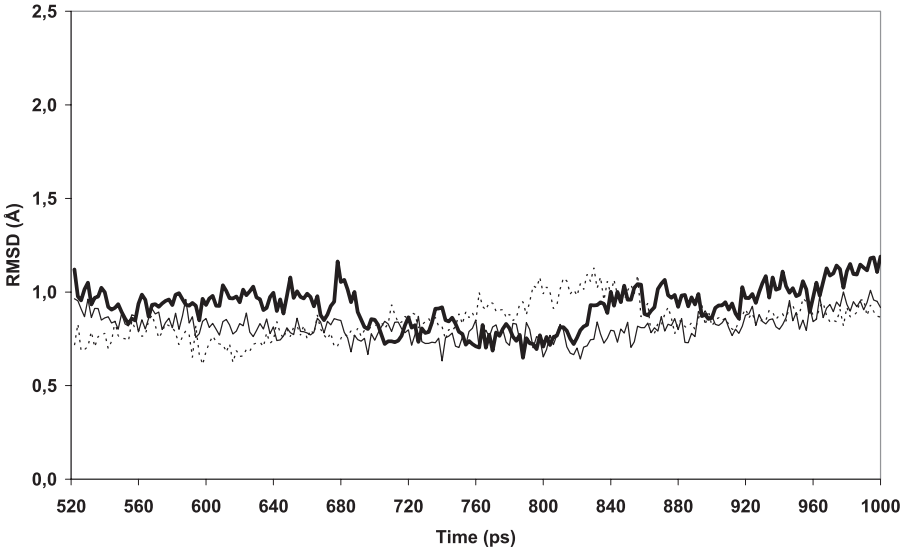

FIGURE 2. **Evolution of the root mean square deviations (*RMSD*) of the Cα atoms with respect to the calculated average structure.** *Thick line*, CCK2R°; *thin line*, CCK2R* in the absence of ligand; *dotted line*, CCK2R* in the presence of CCK. Each *line* is made up of 240 individual points from the last 480 ps of the molecular dynamics trajectory.

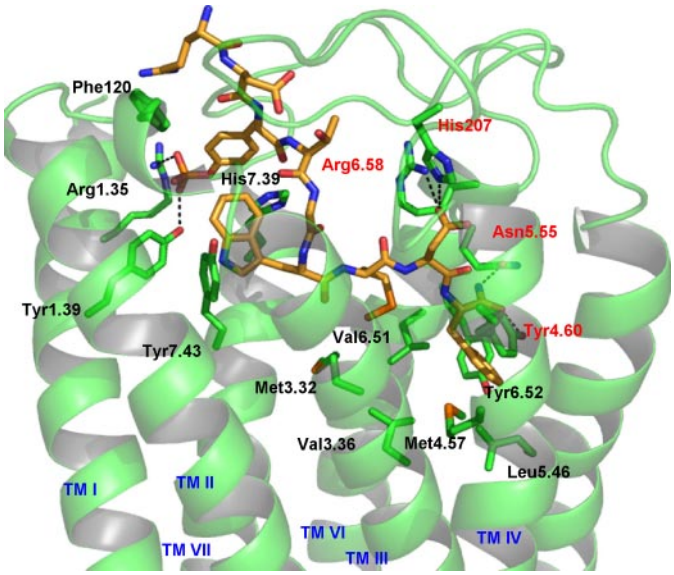

FIGURE 3. ***Schematic representation* of the binding site for CCK in CCK2R.** Side view of the three-dimensional CCK2R*·CCK complex. The CCK2R Cα trace is displayed as a *green ribbon*. For clarity, only amino acid side chains belonging to or close to the binding site are *labeled* and shown as *sticks*. Relevant hydrogen bonds are shown as *dotted lines*. CCK is displayed as *sticks*, and carbon atoms are *colored* in *orange*. Amino acids between which constraints were applied to generate CCK2R* are *labeled* in *red*.

In silico CCK2R° to CCK2R* conversion brought together the upper parts of helices VI and III (Table 2) and caused clockwise rotation of helix VI (observed from extracellular space). Furthermore, in CCK2R*, the cytoplasmic ends of helices VI and VII were more distant from the end of helix III than in CCK2R°, which can be inferred from two distances, one between the Asn-6.55 Cα atom and Ile-156 Cα in IC2 and the other between Cα of Arg-3.50 and Tyr-7.53 (Table 2). More detailed examination of refined CCK2R structures also revealed changes in the position of the side chain of several amino acids and in the nature of contacts, particularly from helices III, IV, V, VI, and VII. Most striking was the rearrangement of the molecular network accompanying rotation of conserved Trp-6.48 from a position inside the binding pocket in CCK2R° to a position outside this binding pocket in CCK2R* (Fig. 4). In fact, in the resting state, Trp-6.48 interacted with Val-3.36, Met-3.32, Ser-7.45, Phe-6.44, and Val-6.51. In CCK2R*, Trp-6.48 no longer interacted with the aforementioned residues, except Phe-6.44, but established new interactions, such as those with Tyr-6.52 and Phe-5.47 (Fig. 4, *A* and *B*). Another consequence of rotation and tilting of helix VI during activation was that Cys-6.47 and Val-6.51 were located in the binding pocket and occupied the previous position of Trp-6.48 in CCK2R°.

Regarding helix IV, although its movement was small, its extracellular end was brought closer to that of helix VI as a result of its rotation and tilting. Indeed, in CCK2R*, Tyr-4.60 formed a hydrogen bond with Asn-6.55, whereas in CCK2R°, Tyr-4.60 established contacts with Met-4.57 and Leu-5.42 (Fig. 4*C*).

Concerning helix V, comparison of the CCK2R* and CCK2R° structures suggested that this helix underwent a concerted movement to allow helix VI to rotate clockwise during activation. In fact, in CCK2R*, Trp-6.48 and Tyr-6.52 have moved to positions previously occupied by Phe-5.47 and Leu-5.43, respectively, in CCK2R° (Fig. 4*D*).

Finally, helix VII was positioned 2 Å higher in CCK2R* relative to CCK2R°. This motion disrupted a network of interactions present in CCK2R° between Tyr-7.43, His-7.39, and Met-3.32. All of these observations suggested that interhelical contacts described above between helices III, IV, V, VI, and VII may be critical for CCK2R activation.

Delineation of the CCK2R° to CCK2R Conversion by Targeted Molecular Dynamics Simulations*—The comparison between modeled structures of CCK2R° and CCK2R* suggested that observed changes in amino acid and helix positions are part of the activation mechanism of CCK2R. However, these data could not answer the questions of how, at a molecular level, the changes involving movements of helices and amino acids actually proceed, in which order they occur, and how they are coordinated. To answer these questions, TMD, an *in silico* method that can simulate intricate conformational changes in proteins as the pathway between two conformations, was applied to CCK2R (27).

In these *in silico* experiments, we observed that a force constant of 0.50 kcal mol^{-1} $Å^{-2}$ over 500 ps was sufficient to achieve the CCK2R° to CCK2R* conversion, as can be inferred from the final value of the r.m.s. deviation of the backbone atoms. The TMD showed that the rotation of the side chain of Trp-6.48 is a consequence of a completed coordinated tilting

and rotation of helix VI and movement of helix V. As a criterion for the tilting of helix VI, two distances, the first one between the Cα carbons of Asn-6.55 and Tyr-189 (not shown) and the second one between the Cα carbons of Val-6.51 and Met-3.32, respectively, were monitored. The latter also allowed measurement of rotation of helix VI, whereas the rotation of the Trp-6.48 side chain was followed by the Chi1 torsion angle. We found that the tilting and rotation movement of helix VI was progressive, as can be deduced from the evolution of the Val-6.51 Cα to Met-3.32 Cα distance (Fig. 5). Furthermore, conformational transition of Trp-6.48 side chain from *g*+ to *t* was not direct; actually, as shown in Fig. 5, an intermediate of −120° was maintained from 260 to 420 ps of simulation. This intermediate state was reached after 260 ps of simulation and occurred once hydrogen bonding interaction between the indole of Trp-6.48 and the Ser-7.45 hydroxyl started to be disrupted, an event that was simultaneous with the beginning of movement of the upper part of this helix. In other words, the hydrogen bonding interaction between Trp-6.48 and Ser-7.45 impeded rotation of Trp-6.48, and the movements of helix VI and VII appeared partially coordinated. Visual inspection of the conformation changes also revealed that the position of helix V was responsible for the stabilization of the intermediate state. Indeed, from 1 to 260 ps, helix V moved but not sufficiently to accommodate the position of helix VI in the active state. At 420 ps, Phe-5.47 and Leu-5.43 reached their final position in the active state, and Trp-6.48 could complete its rotation to occupy its disposition parallel to the membrane (Fig. 6). The targeted molecular dynamics also revealed an important role for Tyr-6.52 in relation to coordination of helix V and VI movements. The tilting movement undergone by the extracellular end of helix VI from 1 to 125 ps appeared to be sufficient to locate Tyr-6.52 in the position occupied by Phe-5.47 in CCK2R°. Thus, at this time, Phe-5.47 had already moved to an orientation close to that of the active one. This suggests that Tyr-6.52 acts as a wedge in the coordinated rotation of Phe-5.47 and Trp-6.48 and, as a consequence, in the coordinated movements of helices V and VI. At last, TMD confirmed that helix III did not significantly move during CCK2R° to CCK2R* conversion, a result in agreement with the constraining hydrophobic interactions of Trp-6.48 with Met-3.32 and Val-3.36, which were disrupted only once rotation of Trp-6.48 was completed (at 460 ps). A schematic representation of helix movements occurring during CCK2R activation is shown in Fig. 7.

TABLE 2

Interhelical distances in the CCK2R* and CCK2R° conformations

Mean distances ± S.D. of the interhelical contacts measured in the production part of the MDs in an explicit membrane (in Å).

	CCK2R*·CCK complex	CCK2R*	CCK2R°
	Å	Å	Å
Ile-156 Cα Arg-6.35 Cα	18.3 ± 0.5	17.3 ± 0.5	15.6 ± 0.4
Arg-3.50 Cα Tyr-7.53 Cα	18.2 ± 0.5	18.4 ± 0.4	17.2 ± 0.3
Val-6.51 Cα Met-3.32 Cα	9.1 ± 0.3	8.8 ± 0.3	11.9 ± 0.5
Val-6.51 Cα Val-3.36 Cα	8.3 ± 0.6	8.2 ± 0.4	12.3 ± 0.5
Tyr-4.60 Cα Asn-6.55 Cα	13.3 ± 0.5	10.7 ± 0.5	15.5 ± 0.8
Tyr-4.60 OH Asn-6.55 OD1	6.5 ± 0.5	3.1 ± 0.4	8.2 ± 0.7
Tyr-7.53 OH Asn-1.50 OD1	2.8 ± 0.1	2.8 ± 0.1	11.0 ± 0.3
Asp-2.50 OD2 Asn-1.50 ND2	2.9 ± 0.1	3.6 ± 0.7	5.8 ± 0.6
Asp-2.50 OD2 Asn-7.49 ND2	3.0 ± 0.2	3.1 ± 0.3	2.9 ± 0.2

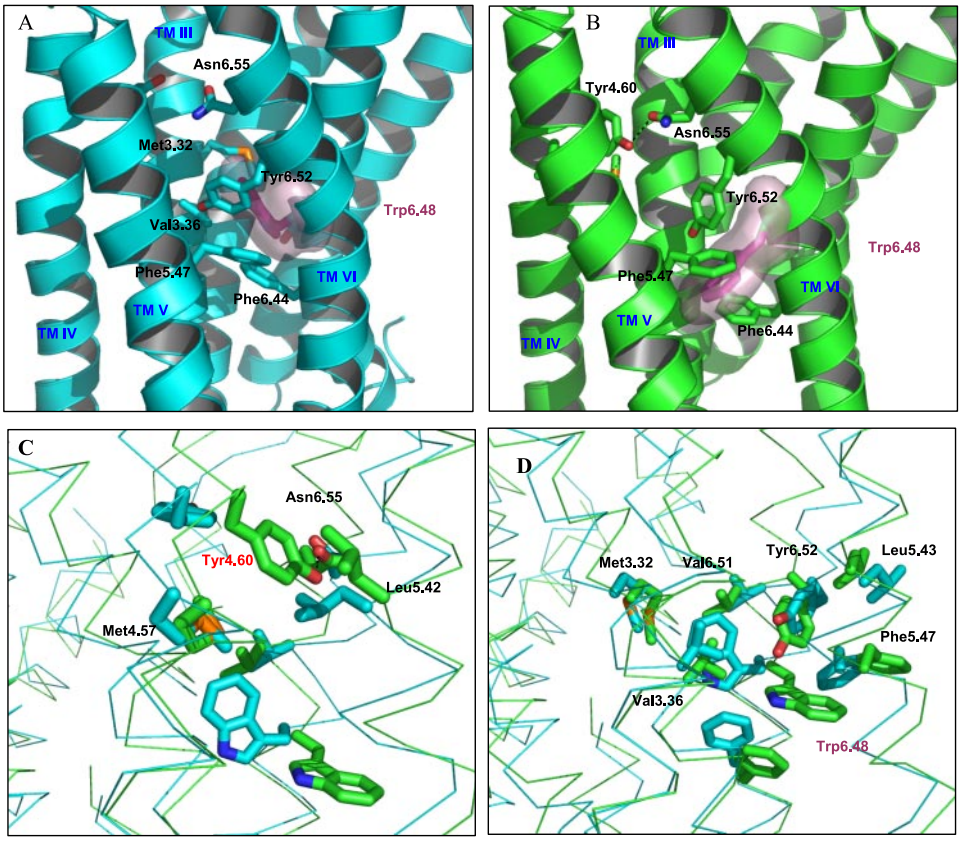

FIGURE 4. **Changes in networks in CCK2R° and CCK2R* conformations.** The models presented here were extracted from averaged minimized structures obtained from the last 250 ps of the simulations. *A* and *B*, detail showing the position of Trp-6.48 and its neighboring residues, in unoccupied CCK2R° (*A*, *cyan*) and CCK2R* (*B*, *green*), respectively. The Cα trace is shown as a *ribbon*, Trp-6.48 is enveloped by a semitransparent solvent-accessible surface *colored* in *pink*, and the interacting residues are displayed as *sticks*. The hydrogen bond between Tyr-4.60 and Asn-6.55 is displayed. *C* and *D*, superposition of inactive (CCK2R°) and active (CCK2R*) conformations *colored* in *blue* and *green*, respectively. For clarity, important amino acids are displayed in *two separated panels*. Relocation of amino acids in the helix V-VI interface discussed under "Discussion" is shown. Note that in the CCK2R* conformation, Trp-6.48 occupied the position of Phe-5.47 in the inactive sate.

Experimental Evidence for the Importance of Aromatic/Hydrophobic Residues in the CCK2R Activation—To verify the role of the aforementioned residues in the activation mechanism, they were mutated, and the basal activities of the resulting mutants were determined by measuring inositol phosphate production in transfected COS-7 cells in the absence of agonist stimulation (basal activity) and the presence of CCK. By doing so, we expected that mutation of amino

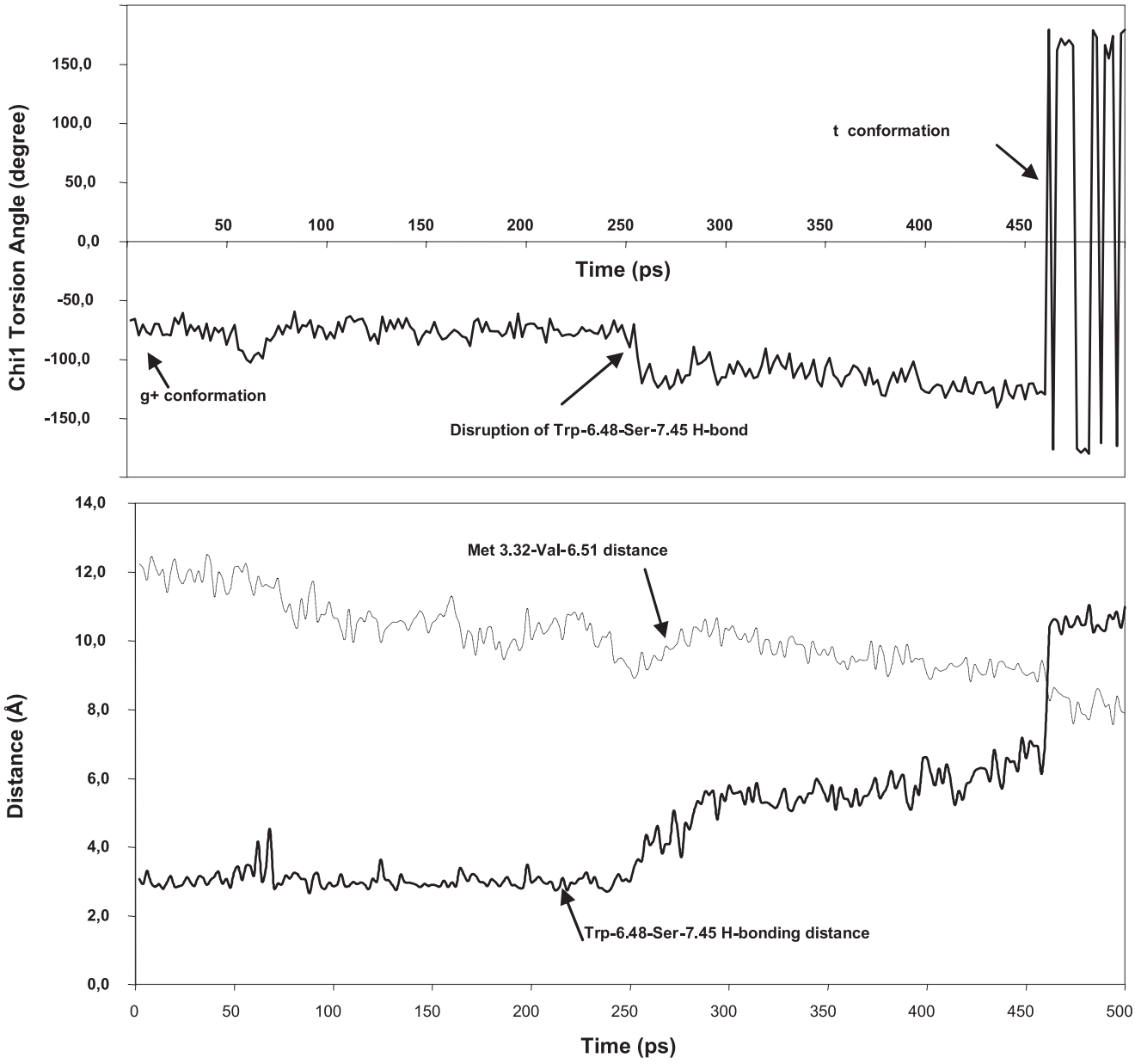

FIGURE 5. **Targeted molecular dynamics applied to conversion of CCK2R° to CCK2R*.** *Top*, time evolution along the TMD simulations of the Chi1 torsion angle of Trp-6.48. *Bottom*, distance between the Cα carbons of Val-6.51 and Met-3.32 (*dotted upper line*) and hydrogen bonding distance between Trp-6.48 and Ser-7.45 (*thick lower line*). Note that there is a correlation between the disruption of the hydrogen bond and the change in the torsion angle of Trp-6.48.

acids that stabilize the receptor in the inactive state should generate constitutively active mutants, whereas mutation of amino acids involved in intramolecular interactions stabilizing the active form should produce mutants devoid of basal activity. As illustrated in Fig. 8, exchange of Val-3.36, Met-4.57, Leu-5.42, Leu-5.43, Phe-5.47, and Trp-6.48 with an Ala yielded constitutively active mutants, indicating that these amino acids are required for stabilization of CCK2R°. Strikingly, mutants V3.36A, L5.42A, L5.43A, and F5.47A displayed robust constitutive activities, since inositol phosphate production in cells transfected with these mutants represented 3–4-fold that of cells transfected with wild-type CCK2R. Mutant W6.48A exhibited a 2.5-fold enhanced activity relative to wild-type CCK2R. Mutant M3.32A and Y7.43A showed a slight or a marked constitutive activity, respectively. For comparison, mutation E3.49A in the conserved (E/D)RY motif, previously found to cause oncogenic activity of the CCK2R, showed a 2-fold increased activity relative to the wild-type CCK2R (26). In contrast, mutation of Tyr-4.60, Phe-6.44, Asn-6.55, and Tyr-6.52 produced CCK2R mutants that exhibited no detectable or significantly lower basal activity than that of wild-type CCK2R, thus ascribing a role in the stability of the active state of the receptor to these amino acids. On the other hand, mutation of Ser-7.45 and His-7.39 did not change basal activity of CCK2R.

The consistency between biological data and structural changes during the CCK2R° to CCK2R* transition was examined. Biological data showing constitutive activity of mutants W6.48A, V3.36A, and M3.32A support the view deduced from analysis of the modeled CCK2R° structure that interactions between Trp-6.48 and Val-3.36/Met-3.32 in

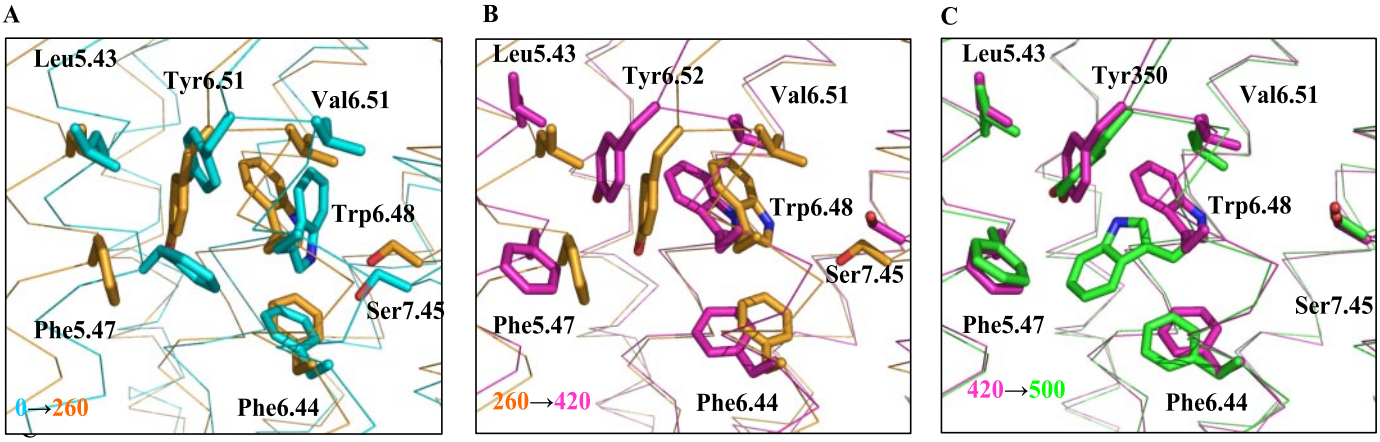

FIGURE 6. **Delineation of CCK2R° to CCK2R* conversion by targeted molecular dynamics simulation.** Overlay of representative snapshots of the TMD trajectory showing the evolution of positions of amino acids from transmembrane helices during CCK2R° to CCK2R* conversion. Transmembrane helices are represented as *ribbons*, and, for clarity, only the side chain of some residues involved in CCK2R activation, Leu-5.43, Phe-5.47, Trp-6.48, Val-6.51, Ser-7.45, and Tyr-6.52 are shown as *sticks*. The *color code* (*blue* → *orange* → *pink* → *green*) corresponds to structures at 0, 260, 420, and 500 ps of simulation, respectively. *A*, 0 and 260 ps; *B*, 260 and 420 ps; *C*, 420 and 500 ps.

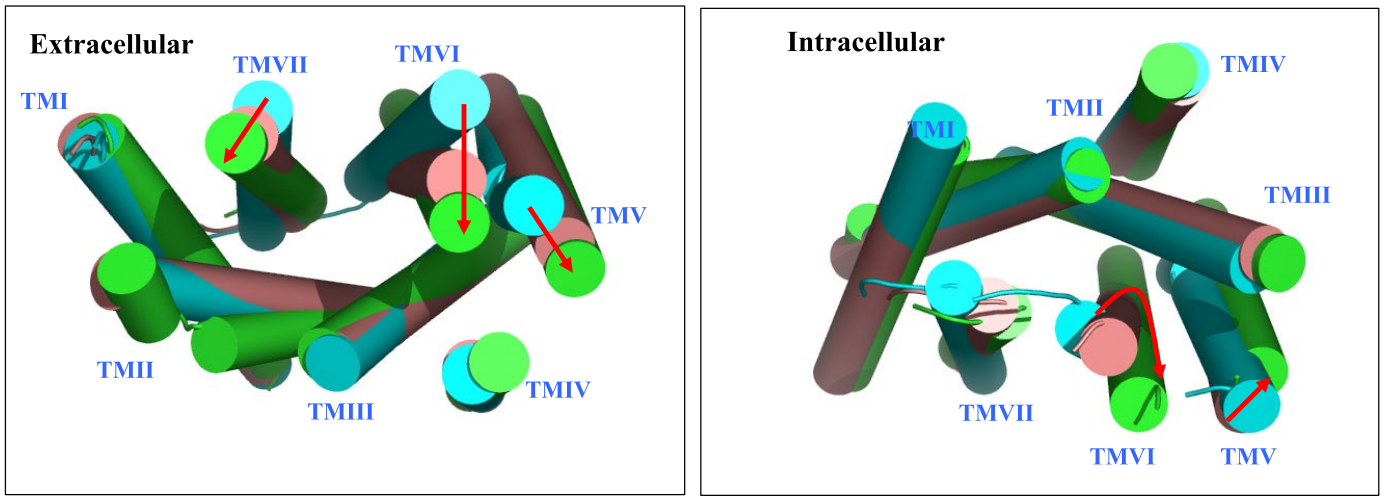

FIGURE 7. **Schematic representation of helix movements during the transition from CCK2R° to CCK2R*.** For clarity, transmembrane helices (*TM*) are shown as *cylinders*. *Blue* corresponds to inactive state (CCK2R°), *pink* to an intermediate conformation (taken at 200 ps) between CCK2R° and CCK2R*, and *green* to the active state (CCK2R*) obtained from the TMD. *Red arrows* indicate movements of helices.

CCK2R° stabilize this state. The biological data also suggest that Leu-5.42 and Leu-5.43, which do not interact with Trp-6.48 in CCK2R°, play a role in the maintenance of the inactive state. To explain this result, we suggest that Leu-5.43 and Phe-5.47 maintain CCK2R in its inactive state, because the motion of these two residues is required for, and must precede, rotation of Trp-6.48 and Tyr-6.52. It is also worthy to note that mutation of Ser-7.45, which appeared to be hydrogen-bound with Trp-6.48, did not produce a constitutive CCK2R, indicating that disruption of a hydrogen bond was not sufficient for CCK2R° to CCK2R* conversion. This result fits with the view that an intermediate state was generated by hydrogen bond disruption.

The finding that Y4.60F and N6.55A mutants lack basal activity fits with the view that the hydrogen bonding interaction between these two residues is important for the stability of CCK2R* conformation. The hydrogen bond between Tyr-4.60 and Asn-6.55 in CCK2R* appears possible because the Tyr-4.60 side chain has moved to occupy the position of Leu-5.42 in the CCK2R*, pushing it outside of the binding pocket. As a consequence, interaction between Met- 4.57 and Leu-5.42 is disrupted during CCK2R° to CCK2R* conversion. The roles of Met-4.57 and Leu-5.42 in the maintenance of the CCK2R° conformation may be explained in this way. At last, pharmacological experiments were carried out with all mutants to measure their expression level, their binding properties, and their ability to respond to CCK stimulation. A summary of results from these experiments is presented in Table 3.

DISCUSSION

In this work, using in parallel state-of-the-art molecular modeling and site-directed mutagenesis approaches, the molecular mechanism of CCK2R activation was investigated with respect to the activation of phospholipase C by measuring inositol phosphate production. A number of amino acids that participate in the activation of CCK2R by stabilizing either active or inactive conformations of the receptor were identified, and a global mechanism of activation involving several key

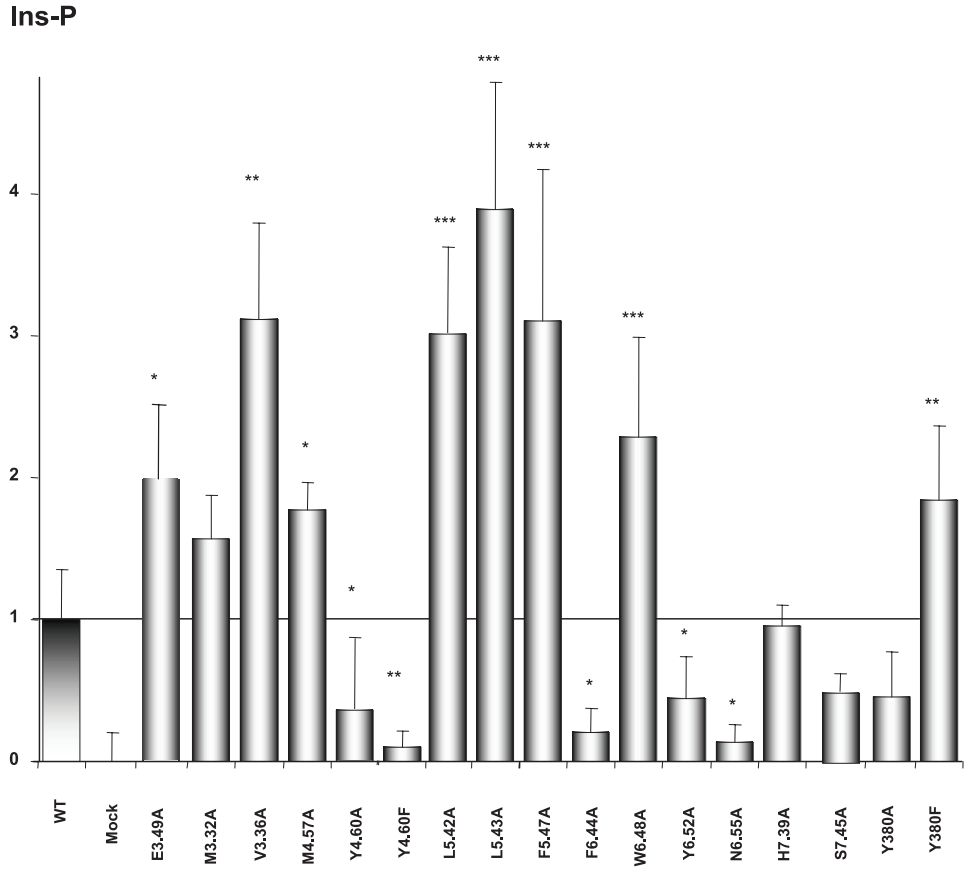

FIGURE 8. **Effect of mutation of hydrophobic/aromatic residues on basal activity of CCK2R.** Basal inositol production in COS-7 cells transiently expressing wild-type (*WT*) or mutated CCK2R. The value 0 represents basal inositol phosphate production in cells transfected with mock plasmid, and it corresponds to about 300 dpm. The value 1 represents basal inositol phosphate production in cells expressing the wild-type CCK2R, and it corresponds to about 650 dpm. Values are calculated for 1 pmol of CCK2R variants as measured by binding experiments. *, $p < 0.05$; **, $p < 0.01$; ***, $p < 0.001$. Mutants that exhibit a significantly higher basal activity are considered to be constitutively active. CCK-induced maximal production of inositol phosphates in COS-7 cells transiently expressing wild-type or mutated CCK2R is reported on Table 3. Values are the means of 3–12 separate determinations.

amino acids within or near the binding site as well as movements of transmembrane helices IV, V, VI, and VII was deduced. We considered that CCK2R, like other G protein-coupled receptors, naturally exists in an equilibrium between receptors in the inactive conformation and receptors in active conformation, the latter being responsible for constitutive activity of the receptor. Previously, we demonstrated that wild-type human CCK2R displays such a constitutive activity, since it enhances production of inositol phosphates in COS-7 cells to a level that is directly a function of the level of receptor expression at the cell surface (18). As demonstrated with other GPCRs, we presumed that adequate mutation of amino acids critical for the stabilization of the inactive state should generate constitutively active mutants, whereas the mutation of amino acids critical for the stabilization of the active state should yield a receptor with zero or decreased basal activity. According to this model, amino acids that appear to be involved in stabilization of CCK2R° are Met-3.32, Val-3.36, Met-4.57, Leu-5.42, Leu-5.43, Phe-5.47, and Trp-6.48, whereas those that stabilize CCK2R* are Tyr-4.60, Phe-6.44, Tyr-6.52, and Asn-6.55. Importantly, all analyzed mutants retained a good ability to respond to the full agonist CCK. On the other hand, constitutively active mutants displayed an activity that remained moderate relative to the maximal CCK-induced response.

One of the most significant structural changes occurring during CCK2R activation concerns helix VI, which undergoes a clockwise rotation where the extracellular end is tilted toward helix III. Targeted molecular dynamics revealed that helix VI movement is coordinated with rotation of helix V and upper movement of helix VII. As a consequence of these movements, interhelical contacts change from the inactive to active state, the most remarkable being the molecular network around the conserved Trp-6.48.

Since the above mechanism of CCK2R activation was deduced from the *in silico* conversion of CCK2R° to empty CCK2R* and the role of the agonist is to stabilize CCK2R*, the consistency of this activation mechanism with the mode of CCK binding to CCK2R* must be considered. In helix VI, Arg-6.58 and Asn-6.55 participate in CCK binding. In empty CCK2R*, the Arg-6.58 guanidium is associated with water molecules, whereas Asn-6.55 is in tight interaction with the Tyr-4.60 hydroxyl and thus contributes to CCK2R* stabilization. In the presence of CCK, the Arg-6.58 guanidium moves slightly toward the binding cavity to interact with the side chain of CCK-aspartic acid. Interestingly, following CCK binding, the Asn-6.55–Tyr-4.60 bond dissociates, leaving the side chains of these amino acids free to accommodate the CCK amide through hydrogen bonds. As for CCK-Trp, its location between helix III and VII through interactions with His-7.39 and Tyr-7.43 contributes to the stabilization of helix VII in the upper position as found in empty CCK2R*. In the absence of CCK, in CCK2R*, helix VII position is locked by interactions between His-7.39 and Tyr-7.43 with Met-3.32. Furthermore, in CCK2R* an aromatic/hydrophobic pocket is enlarged due to the rotation of amino acids surrounding Trp-6.48. CCK-Phe perfectly accommodates, in this binding pocket formed by Val-3.36, Met4.57 and Tyr4.60, Leu5.46, and Val6.51 and Tyr6.52 and thus contributes to the stabilization of CCK2R*. Several amino acids critical for CCK2R activation, such as Trp-6.48, Leu-5.42, Leu-5.43, and Phe-5.47, are not in contact with CCK, since their side chains are directed outside the binding cavity in CCK2R. All together, these data provide an original picture of how CCK2R can adopt the active conformation on its own, with an energy barrier between active and inactive conformations that

TABLE 3

Pharmacological properties of CCK2R mutants

Binding properties and biological potency of mutated CCK2R were determined as described under "Experimental Procedures." Mutation factors (F) were calculated as K_d (mutated CCK2R)/K_d (WT-CCK2R) or EC_{50} (mutated CCK2R/EC_{50} (WT-CCK2R). E_{max} values are expressed in percentage of wild-type CCK2R maximal inositol accumulation in response to 1 μM CCK. Results represent the means ± S.E. of at least three independent experiments performed in duplicate on separately transfected COS-7 cells.

CCK2R	CCK binding						CCK-induced inositol phosphate production		
	High affinity		Low affinity		B_{max}		EC_{50}	F_{mut}	E_{max}
	K_{d1}	F_{mut1}	K_{d2}	F_{mut2}	High affinity	Low affinity			
	nM		nM		pmol/10^6 cells		nM		
Wild type	0.37 ± 0.02	1	2.8 ± 0.3	1	0.89 ± 0.05	2.3 ± 0.2	0.34 ± 0.05	1	100
R1.35A	1.30 ± 0.30	4	22.0 ± 3.0	8	0.19 ± 0.04	0.66 ± 0.05	2.2 ± 0.4	6	100
Y1.39A	0.12 ± 0.03	0.3	6.0 ± 2.6	1.7	0.41 ± 0.12	2.5 ± 1.1	0.34 ± 0.02	1	96
F120A	1.20 ± 0.20	3	17.0 ± 4.0	6	0.14 ± 0.03	0.65 ± 0.05	1.6 ± 0.2	5	99
M3.32A	0.23 ± 0.09	0.6	42.8 ± 20.9	12.0	1.40 ± 0.80	4.5 ± 1.3	O.43 ± 0.11	1	119
V3.36A	0.10 ± 0.03	0.3	6.6 ± 2.3	1.8	0.46 ± 0.07	2.2 ± 0.6	0.53 ± 0.14	1.3	90
M4.57A	0.46 ± 0.05	1.3	73.9 ± 59.9	20.8	0.19 ± 0.05	1.19 ± 0.47	0.90 ± 0.18	2.2	121
Y4.60F	3.20 ± 0.50	9	21.0 ± 4.0	8	0.28 ± 0.05	0.82 ± 0.18	3.7 ± 0.4	11	97
Y4.60A	50.0 ± 5.0	136	436 ± 24	156	0.45 ± 0.05	2.2 ± 0.5	37.0 ± 6.0	109	215
H207A	8.30 ± 1.40	27	51.0 ± 5.0	18	0.31 ± 0.05	0.78 ± 0.13	12.0 ± 2.0	35	90
L5.42A	0.20 ± 0.02	0.6	4.0 ± 0.8	1.1	0.54 ± 0.04	3.3 ± 0.2	0.48 ± 0.07	1.2	190
L5.43A	0.30 ± 0.04	0.8	32.1 ± 17.5	9.0	2.40 ± 0.60	3.8 ± 2.0	0.39 ± 0.07	0.9	120
F5.47A	0.31 ± 0.05	0.9			1.54 ± 0.28		0.27 ± 0.06	0.7	150
F6.44A	0.22 ± 0.05	0.6	14.2 ± 7.2	4.0	0.58 ± 0.13	0.77 ± 0.30	0.38 ± 0.07	0.9	96
W6.48A	0.31 ± 0.05	0.9	19.5 ± 9.2	5.5	0.60 ± 0.09	3.0 ± 1.5	0.75 ± 0.17	1.8	172
V6.51A	0.28 ± 0.09	0.8	15.0 ± 6.9	4.2	0.34 ± 0.09	1.5 ± 0.4	0.40 ± 0.11	1.2	102
Y6.52A	0.25 ± 0.05	0.7	3.9 ± 1.6	1.0	0.63 ± 0.13	2.4 ± 0.8	0.32 ± 0.09	0.8	127
N6.55A	12.0 ± 1.0	32	114.0 ± 5.0	41	0.17 ± 0.06	0.62 ± 0.04	11.0 ± 1.0	32	89
R6.58A	28.0 ± 2.0	76			0.49 ± 0.04		22.0 ± 4.0	65	100
H7.39A	0.56 ± 0.20	1.5	18.3 ± 1.2	5.2	0.07 ± 0.06	1.7 ± 1.4	2.84 ± 0.57	6.8	90
Y7.43A	0.92 ± 0.27	2.6	53.1 ± 12.4	14.9	0.32 ± 0.09	1.5 ± 0.5	1.18 ± 0.21	1.2	104
Y7.43F	0.29 ± 0.14	0.8	29.0 ± 21.1	8.1	0.80 ± 0.32	9.3 ± 5.2	0.52 ± 0.03	1.2	140
S7.45A	0.73 ± 0.10	2.0			1.80 ± 0.09		0.24 ± 0.09	0.7	75

is probably small. Furthermore, they show how the peptide agonist, CCK, binds to CCK2R* to stabilize it through specific interactions, some of which concern anchoring points, whereas others serve to maintain helices at critical positions in CCK2R*.

The above global structural changes observed during CCK2R activation are in line with those described or suggested with other GPCRs using biochemical and biophysical techniques, but they appear quantitatively smaller (28–30). Concerning movements of helix VI, pioneering studies using electron paramagnetic resonance analysis of spin-labeled rhodopsin have revealed the proximity of helices III and VI and rigid body movement of helix VI upon light activation (31). This was confirmed by Cys cross-linking and metal-ion binding of these helices, which prevent activation of the rhodopsin-coupled G protein, transducin (31, 32). It is worthy of mention that the strategy of engineered metal-ion binding sites between transmembrane helices applied to a number of peptide receptors confirmed the proximity of the upper part of helices III and VI and their relative motion during receptor activation (33). Interestingly, the maximal efficacy of metals was obtained when the metal ion site was formed by amino acids in positions III:08 and VI:16, which correspond to Met-3.32 and Val-6.51 of CCK2R, respectively. A distance of about 8 Å between the Cα carbons of these two residues was found in CCK2R*, a value that is in agreement with the optimal distance required for metal coordination. Using a cysteine-reactive fluorophore incorporated into mutants of a G_s-coupled GPCR, the β_2-adrenoreceptor, movements of the cytoplasmic sides of helices III and VI, relative to the membrane lipid bilayer, were directly detected upon agonist activation (34). Data obtained with two GPCRs having distant amino acid sequences, the β_2-adrenoreceptor and the parathyroid hormone receptor, suggested that the activation mechanism that requires relative movement of helices III and VI to one another is conserved among GPCRs (32). The specific role of the conserved Trp of the motif CW*X*PFF in helix VI (Trp-6.48 in CCK2R) as a rotamer switch for GPCR activation has been elegantly documented in rhodopsin using solid-state magic angle spinning NMR measurements of rhodopsin and metarhodopsin II (23). It was indeed shown that interactions between the retinal and Trp-265 of rhodopsin contributes to the maintenance of rhodopsin in the inactive state in the dark, whereas disruption of this interaction under light activation allows Trp-265 and helix VI to rotate and adopt the active conformation (23). It was also demonstrated with metarhodopsin II that the packing interaction between Trp-265 and Gly-121 is disrupted, a result consistent with motion of helix VI away from helix III. In the current study with CCK2R, we observed an increase of the distance between equivalent amino acids, namely Trp-6.48 and Val-3.36 (23).

Concerning helix V, which undergoes a concerted rotation with helix VII during CCK2R activation, identification of Phe-5.47 as a key residue is in line with the concept that a conserved Phe/Tyr residue in this helix (located at −3 residues of a proline and corresponding to Phe-5.47 in CCK2R) plays a critical role in the activation switch. In ghrelin and β_2-adrenergic receptors, mutation of this residue has been reported to decrease receptor activity (30). Surprisingly, the mutation of Phe-5.47 in CCK2R yielded a constitutively active receptor, and both TMD and experimental results clearly ascribed a constraining role to helix V, since the motion of Phe-5.47 and Leu-5.43 liberates the space that allows Trp-6.48 and Tyr-6.52 to rotate.

With respect to helix VII, its role as an activation or coupling

switch has been illustrated. For instance, in the C5a receptor, motion of helix VII has been proposed to explain the activation switch observed with mutants (35). Movement of the cytoplasmic interface of this helix during activation is supported by data showing that the NP*XX*Y motif is accessible to an antibody in metarhodopsin, whereas it is not in rhodopsin maintained in the dark (36). Furthermore, it has been shown that upon formation of metarhodopsin, the salt bridge between Glu-113 in helix III and the protonated Schiff base formed by retinal and Lys-296 in helix VII is disrupted, which requires movement of helix VII relative to helix III (37). In CCK2R, we have noticed an upper movement of helix VII of about 2 Å. Such a movement, if applied to rhodopsin helix VII, would cause disruption of the Glu^{113}–Lys^{296} salt bridge and would probably establish contact between Lys^{296} and Glu^{181} (37). TMD with CCK2R showed that the upper movement of helix VII starts once the Trp-6.48 side chain has begun to rotate and the hydrogen bonding interaction with Ser-7.45 is lost. Disruption of the hydrogen bond may be an important event in the activation process of CCK2R, but the fact that mutation of Ser-7.45 did not generate constitutive activity also indicated that disruption of this hydrogen bond is not sufficient for CCK2R activation. Asn-7.45 in histamine H1 receptor, the cognate residue of Ser-7.45, was reported to play a role in receptor activation (38). Indeed, it was demonstrated that in the H1 receptor, Asn-7.45 constrained Trp-6.48 in the inactive *g*+ conformation through a hydrogen bonding interaction and that, unlike in CCK2R, disruption of this hydrogen bond by leucine substitution leads to a constitutively active receptor (38).

The critical role of helix IV in CCK2R activation is remarkable. This helix does not undergo significant movement during CCK2R°-CCK2R* conversion, but its distance with respect to helix VI seems critical in CCK2R*, as supported by the dramatic decrease of the distance between the two helices in CCK2R* relative to the CCK2R° and the role played by the CCK-amide in the maintenance of this proximity. Helix IV may therefore be considered a part of the rigid body of the receptor and contributes to the correct positioning of helix VI. The importance of helix IV as an anchoring point for peptidic ligand binding has been documented for other peptide receptors. In the CXCR4 chemokine receptor, urotensin II receptor, vasopressin V1a receptor, and melanocortin-4 receptor, the residue equivalent to Tyr-4.60 in CCK2R is critical for agonist binding (39–42). However, with the current work on CCK2R, this is the first example of a key role being ascribed to helix IV in the control of the equilibrium between inactive and active conformations.

Taken together, structural changes observed during CCK2R activation are in line with those described or suggested with other GPCRs using biochemical and biophysical techniques, but they appear quantitatively smaller (28–30). Instead, changes that accompany CCK2R activation are quantitatively more comparable with those deduced from the recent crystallization of a photoactivated, deprotonated intermediate of rhodopsin (43). Furthermore, our data point out that the role played by some conserved amino acids in the activation process is different in CCK2R relative to other members of the GPCR family A. Hence, during activation, CCK2R undergoes conformational changes that are shared by members of GPCR class A but also appears to present divergent features, which may account for its ligand and signaling selectivity. In the future, studies on GPCR mechanism of activation will have to take into account the entire structure of the receptor, including the third intracellular loop, the structure of which is dependent on the relative position of helices V and VI as well as on binding of the α subunit of the coupled G-protein.

It is worthy of note that several amino acids identified as critical in the activation process of CCK2R have been previously mutated. For instance, the exchange of Met-3.32, Val-3.36, and Leu-5.43 was shown to increase basal activity of CCK2R in COS-7 cells (24, 44). Interestingly, in the mentioned studies, partial agonist activity of PD-135,158, a molecule initially believed to be an antagonist, was increased on M4.57A and W6.48A mutants, whereas it disappeared on F5.47A and Y6.52A mutants. Such mutants were previously defined as "a subgroup of activating mutations which facilitates receptor isomerization to the active state and in parallel perturbs ligand receptor interactions" (44). Our data provide a significant advance, since they show how CCK2R can adopt the active conformation on its own and how the peptide agonist, CCK, binds to CCK2R* to stabilize it. Obviously, additional works using biochemical and biophysical approaches are highly desirable to further verify the findings of the present study.

Last, this study with CCK2R illustrates how TMD, in contrast to ordinary molecular dynamics simulation, is a powerful molecular modeling technique able to study conformational conversion between inactive and active states of a complex membrane protein such as a GPCR. Previously, TMD has been successfully applied to study conformational transitions of KcsA channel, chymotrypsin, and other proteins (27, 45, 46). However, to our knowledge, analysis of CCK2R activation represents the first successful application of TMD to a GPCR. Based on the findings from this study, TMD appears appropriate to study, at the atomic level, the structural determinants involved in the activation of a GPCR. Interestingly, the intermediary receptor structures that can be identified and extracted from the TMD trajectories can be used as targets for ligand docking studies. Besides providing information of basic scientific interest, it is expected that insight into the activation and inactivation mechanism of GPCRs will be exploited in structure-based drug discovery efforts.

Acknowledgment—We sincerely thank the Centre Informatique National de l'Enseignement Supérieur (Montpellier, France) for software and hardware support.

REFERENCES

1. Lefkowitz, R. J., Cotecchia, S., Samama, P., and Costa, T. (1993) *Trends Pharmacol. Sci.* **14,** 303–307
2. Bond, R. A., and Ijzerman, A. P. (2006) *Trends Pharmacol. Sci.* **27,** 92–96
3. Kenakin, T. (1995) *Trends Pharmacol. Sci.* **16,** 256–258
4. Dufresne, M., Seva, C., and Fourmy, D. (2006) *Physiol. Rev.* **86,** 805–847
5. Kopin, A. S., Lee, Y. M., McBride, E. W., Miller, L. J., Lu, M., Lin, H. Y., Kolakowski, L. F., Jr., and Beinborn, M. (1992) *Proc. Natl. Acad. Sci. U. S. A.* **89,** 3605–3609
6. Wank, S. A., Pisegna, J. R., and de Weerth, A. (1992) *Proc. Natl. Acad. Sci. U. S. A.* **89,** 8691–8695

7. Noble, F., Wank, S. A., Crawley, J. N., Bradwejn, J., Seroogy, K. B., Hamon, M., and Roques, B. P. (1999) *Pharmacol. Rev.* **51,** 745–781
8. Ding, W. Q., Kuntz, S. M., and Miller, L. J. (2002) *Cancer Res.* **62,** 947–952
9. Hellmich, M. R., Rui, X. L., Hellmich, H. L., Fleming, R. Y., Evers, B. M., and Townsend, C. M., Jr. (2000) *J. Biol. Chem.* **275,** 32122–32128
10. Herranz, R. (2003) *Med. Res. Rev.* **23,** 559–605
11. Blevins, G. T., Jr., van de Westerlo, E. M., Yule, D. I., and Williams, J. A. (1994) *J. Pharmacol. Exp. Ther.* **269,** 911–916
12. Schmassmann, A., Garner, A., Flogerzi, B., Hasan, M. Y., Sanner, M., Varga, L., and Halter, F. (1994) *Gut* **35,** 270–274
13. Kopin, A. S., McBride, E. W., Schaffer, K., and Beinborn, M. (2000) *Trends Pharmacol. Sci.* **21,** 346–353
14. Reubi, J. C. (2003) *Endocr. Rev.* **24,** 389–427
15. Gales, C., Poirot, M., Taillefer, J., Maigret, B., Martinez, J., Moroder, L., Escrieut, C., Pradayrol, L., Fourmy, D., and Silvente-Poirot, S. (2003) *Mol. Pharmacol.* **63,** 973–982
16. Langer, I., Tikhonova, I. G., Travers, M. A., Archer-Lahlou, E., Escrieut, C., Maigret, B., and Fourmy, D. (2005) *J. Biol. Chem.* **280,** 22198–22204
17. Silvente-Poirot, S., Escrieut, C., Gales, C., Fehrentz, J. A., Escherich, A., Wank, S. A., Martinez, J., Moroder, L., Maigret, B., Bouisson, M., Vaysse, N., and Fourmy, D. (1999) *J. Biol. Chem.* **274,** 23191–23197
18. Foucaud, M., Tikhonova, I. G., Langer, I., Escrieut, C., Dufresne, M., Seva, C., Maigret, B., and Fourmy, D. (2006) *Mol. Pharmacol.* **69,** 680–690
19. Palczewski, K., Kumasaka, T., Hori, T., Behnke, C. A., Motoshima, H., Fox, B. A., Le Trong, I., Teller, D. C., Okada, T., Stenkamp, R. E., Yamamoto, M., and Miyano, M. (2000) *Science* **289,** 739–745
20. Thompson, J. D., Higgins, D. G., and Gibson, T. J. (1994) *Nucleic Acids Res.* **22,** 4673–4680
21. Fiser, A., Do, R. K., and Sali, A. (2000) *Protein Sci.* **9,** 1753–1773
22. Lin, S. W., and Sakmar, T. P. (1996) *Biochemistry* **35,** 11149–11159
23. Crocker, E., Eilers, M., Ahuja, S., Hornak, V., Hirshfeld, A., Sheves, M., and Smith, S. O. (2006) *J. Mol. Biol.* **357,** 163–172
24. Blaker, M., Ren, Y., Seshadri, L., McBride, E. W., Beinborn, M., and Kopin, A. S. (2000) *Mol. Pharmacol.* **58,** 399–406
25. Kopin, A. S., McBride, E. W., Quinn, S. M., Kolakowski, L. F., Jr., and Beinborn, M. (1995) *J. Biol. Chem.* **270,** 5019–5023
26. Gales, C., Sanchez, D., Poirot, M., Pyronnet, S., Buscail, L., Cussac, D., Pradayrol, L., Fourmy, D., and Silvente-Poirot, S. (2003) *Oncogene* **22,** 6081–6089
27. Compoint, M., Picaud, F., Ramseyer, C., and Girardet, C. (2005) *J. Chem Phys.* **122,** 134707–134715
28. Gether, U. (2000) *Endocr. Rev.* **21,** 90–113
29. Ballesteros, J. A., Shi, L., and Javitch, J. A. (2001) *Mol. Pharmacol.* **60,** 1–19
30. Schwartz, T. W., Frimurer, T. M., Holst, B., Rosenkilde, M. M., and Elling, C. E. (2006) *Annu. Rev. Pharmacol. Toxicol.* **46,** 481–519
31. Farrens, D. L., Altenbach, C., Yang, K., Hubbell, W. L., and Khorana, H. G. (1996) *Science* **274,** 768–770
32. Sheikh, S. P., Vilardarga, J. P., Baranski, T. J., Lichtarge, O., Iiri, T., Meng, E. C., Nissenson, R. A., and Bourne, H. R. (1999) *J. Biol. Chem.* **274,** 17033–17041
33. Elling, C. E., Frimurer, T. M., Gerlach, L. O., Jorgensen, R., Holst, B., and Schwartz, T. W. (2006) *J. Biol. Chem.* **281,** 17337–17346
34. Gether, U., Lin, S., Ghanouni, P., Ballesteros, J. A., Weinstein, H., and Kobilka, B. K. (1997) *EMBO J.* **16,** 6737–6747
35. Gerber, B. O., Meng, E. C., Dotsch, V., Baranski, T. J., and Bourne, H. R. (2001) *J. Biol. Chem.* **276,** 3394–3400
36. Abdulaev, N. G., and Ridge, K. D. (1998) *Proc. Natl. Acad. Sci. U. S. A.* **95,** 12854–12859
37. Ludeke, S., Beck, M., Yan, E. C., Sakmar, T. P., Siebert, F., and Vogel, R. (2005) *J. Mol. Biol.* **353,** 345–356
38. Jongejan, A., Bruysters, M., Ballesteros, J. A., Haaksma, E., Bakker, R. A., Pardo, L., and Leurs, R. (2005) *Nat. Chem. Biol.* **1,** 98–103
39. Gerlach, L. O., Skerlj, R. T., Bridger, G. J., and Schwartz, T. W. (2001) *J. Biol. Chem.* **276,** 14153–14160
40. Boucard, A. A., Sauve, S. S., Guillemette, G., Escher, E., and Leduc, R. (2003) *Biochem. J.* **370,** 829–838
41. Cotte, N., Balestre, M. N., Aumelas, A., Mahe, E., Phalipou, S., Morin, D., Hibert, M., Manning, M., Durroux, T., Barberis, C., and Mouillac, B. (2000) *Eur. J. Biochem.* **267,** 4253–4263
42. Haskell-Luevano, C., Cone, R. D., Monck, E. K., and Wan, Y. P. (2001) *Biochemistry* **40,** 6164–6179
43. Salom, D., Lodowski, D. T., Stenkamp, R. E., Le Trong, I., Golczak, M., Jastrzebska, B., Harris, T., Ballesteros, J. A., and Palczewski, K. (2006) *Proc. Natl. Acad. Sci. U. S. A.* **103,** 16123–16128
44. Beinborn, M., Ren, Y., Blaker, M., Chen, C., and Kopin, A. S. (2004) *Mol. Pharmacol.* **65,** 753–760
45. Matrai, J., Verheyden, G., Kruger, P., and Engelborghs, Y. (2004) *Protein Sci.* **13,** 3139–3150
46. Rodriguez-Barrios, F., Balzarini, J., and Gago, F. (2005) *J. Am. Chem. Soc.* **127,** 7570–7578
47. Meng, E. C., and Bourne, H. R. (2001) *Trends Pharmacol. Sci.* **22,** 587–593
48. Hubbell, W. L., Altenbach, C., Hubbell, C. M., and Khorana, H. G. (2003) *Adv. Protein Chem.* **63,** 243–290
49. Lu, Z. L., Saldanha, J. W., and Hulme, E. C. (2002) *Trends Pharmacol. Sci.* **23,** 140–146